Astronomical Journal, 117, 2381, (1999)

The History of Low-Mass Star Formation in the Upper Scorpius OB Association

Thomas Preibisch
Max-Planck-Institut für Radioastronomie, Auf dem Hügel 69, D-53121 Bonn, Germany; also at Astronomisches Institut, Universität Würzburg, D–97074 Würzburg, Germany; preib@mpifr-bonn.mpg.de

and

Hans Zinnecker
Astrophysikalisches Institut Potsdam, An der Sternwarte 16, D–14482 Potsdam, Germany; hzinnecker@aip.de

ABSTRACT

We use a large sample of about 100 low-mass pre-main sequence (PMS) stars in the Upper Scorpius OB association to explore the star formation history and the IMF of this association. Upper Scorpius is an ideal target for such a study, because the star formation process there is finished. The PMS stars have recently been found in a spatially unbiased wide field survey of X-ray selected stars in a 160 square-degree area, covering the Upper Scorpius association nearly completely. Following the optical characterization of these PMS stars, we present a new HR diagram for this association.

We perform a detailed analysis of the HR diagram, taking proper account of the uncertainties and the effects of unresolved binaries, and derive ages and masses for the PMS stars. We find that the low-mass PMS stars have a mean age of about 5 Myr and show no evidence for a large age dispersion. This agrees very well with the age of 5 – 6 Myr previously found for the massive stars and shows that low-mass and high-mass stars are coeval and co-spatial and thus have formed together.

We conclude that the star formation process in Upper Scorpius was probably triggered by the shock wave of a supernova explosion in the nearby Upper Centaurus-Lupus association. After a short burst of very high star formation activity, which lasted only for a few Myr, star formation in Upper Scorpius was halted, probably by the strong winds and the ionizing radiation of the numerous massive stars which dispersed the molecular cloud.

Subject headings: associations: individual (Scorpius Centaurus) – stars: pre-main sequence – stars: corona – stars: formation – stars: mass function – X-rays: stars

1. Introduction

The knowledge of the stellar content of OB associations is a key towards determining the origin of the initial mass function of field stars (Miller & Scalo 1978; Zinnecker et al. 1993). OB associations and gravitationally unbound clusters are likely to be the dominant birthplaces for the low-mass field star population. While the low-mass stellar population in T associations (like Taurus-Auriga; cf. Kenyon & Hartmann 1995; Neuhäuser 1997 and references therein) or very young clusters (like IC 348; cf. Herbig 1998; Lada & Lada 1995) seems to be rather well-known, not much is known about the low-mass stellar contents of OB associations. The low-mass population in OB associations remains largely unexplored, because most of the low-mass pre-main sequence (PMS) stars cannot be easily distinguished from normal field stars. Only the classical T Tauri stars can be rather easily found by their strong Hα emission, e.g. by objective prism surveys. However, the PMS population is dominated by the weak-line T Tauri stars (cf. Krautter 1996), which lack such an easily detectable signature and thus are very hard to find among the many thousands of foreground and background field stars in the huge area on the sky (several hundred square-degrees) covered by nearby OB associations.

Interestingly, most PMS stars are strong X-ray emitters. Since the young stars rotate rather rapidly, their X-ray luminosities are about 2 – 3 orders of magnitude above those of main sequence stars of similar spectral type (cf. Montmerle 1996). X-ray observations have proven to be extremely efficient in discovering the PMS stars among the older field stars (e.g. Walter et al. 1988; Neuhäuser 1997 and references therein; Preibisch et al. 1998).

The Scorpius Centaurus association is the OB association nearest to the Sun. It contains several hundred B stars which concentrate in the three subgroups Upper Scorpius, Upper Centaurus Lupus, and Lower Centaurus Crux (cf. Blaauw 1964, 1991; de Zeeuw et al. 1999). Upper Scorpius is the youngest subgroup, Upper Centaurus Lupus the oldest subgroup of the association (de Geus et al. 1989). While there are several dark clouds with ongoing star formation in the neighborhood of the Scorpius Centaurus association, especially the ρ Oph molecular cloud (cf. Wilking 1991) to the east and the Lupus dark clouds (cf. Krautter 1991) to the south, there is no evidence for ongoing star formation activity in the Scorpius Centaurus association itself. The lack of dense molecular material and deeply embedded young stellar objects indicates that the star formation process in Upper Sco is over. This makes it an ideal target for an investigation of the IMF, since the stars of all masses are already present and one can study the outcome of the completed star formation process. The area is essentially free of dense gas and dust clouds, and the association members show only very moderate extinctions ($A_V \lesssim 2$ mag). This is probably the consequence of the massive stellar winds and several supernova explosions, which have cleared the region from diffuse matter and created a huge system of loop-like H I structures around the association (cf. de Geus 1992).

The Upper Sco association was very well investigated by the astrometry satellite Hipparcos, yielding astrometric data for 1215 stars. De Zeeuw et al. (1999) investigated the kinematic membership of these stars and could identify 120 members, which we will denote "Hipparcos members" in the following text. The mean distance of these stars as determined from the Hipparcos parallaxes is 145 pc. The ages of the high-mass stars in Upper Sco are well known: De Zeeuw & Brand (1985) and de Geus et al. (1989) independently derived an age of $5-6$ Myr for the B stars from the main sequence turnoff in the HR diagram. The kinematic age of the association, determined by tracing back the motions of the stars until the smallest configuration is reached, is 4.5 Myr (Blaauw 1964). As noted by Brown et al. (1997), this kinematic method tends to underestimate the true age and thus this result is fully consistent with the nuclear age of $5-6$ Myr. We conclude that the age of the high-mass stars in Upper Sco is very reliable. As noted by de Geus et al. (1989), there is no evidence for a significant spread in ages among the high-mass stars.

The first systematic search for low-mass members of Upper Sco was performed by Walter et al. (1994, W94 hereafter), who obtained spectroscopy and photometry for the optical counterparts of X-ray sources detected in 7 individual EINSTEIN fields. W94 classified 28 objects as low-mass PMS stars. By comparison of their locations in the HR diagram with theoretical evolutionary tracks, W94 determined a mean age of (1.2 ± 0.7) Myr for these stars. This would imply that the low-mass PMS stars are significantly younger than the B stars. The small spread of ages can only be understood if the formation of these stars was triggered by some external event. W94 offered two possible explanations for their findings: The first explanation is that there were two separate short episodes of star formation in Upper Sco; a first one forming only high-mass stars and, about 4 Myr later, a second one forming only low-mass stars. In this scenario it would be hard to understand why high-mass and low-mass stars should have formed separately. The alternative scenario proposed by W94 assumes only a single episode of star formation which started some 5 Myr ago. The apparent age difference between the low-mass stars and the high-mass stars is caused by the different kinds of protostellar collapse: while the high-mass stars collapsed quickly by gravitational free-fall, the collapse of the low-mass protostars went through a very slow phase of ambipolar diffusion. While the high-mass stars reached the main sequence after a few 10^5 yr, the low-mass objects remained in a deeply embedded protostellar phase for several Myr. About 3.5 Myr after the onset of star formation the most massive star in the association exploded as a supernova; the shock wave of this explosion dispersed the protostellar cores, causing the low-mass stars to cross the birthline, i.e. get optically visible, and setting their isochronal age to zero.

Martin (1998) used the data of W94 to propose a very different scenario. He did not determine individual stellar ages, but argued that the spread in lithium line widths found by W94 suggest a very large spread of ages among the PMS stars. According to his argument, stellar ages would range from ~ 1 Myr up to $\sim 10 - 20$ Myr. If these ages were true, the locations of the stars in the HR diagram could only be understood if there was a large spread in the stellar distances; the oldest stars would have to be at distances of only $80 - 100$ pc. Furthermore, in this scenario it is hard to understand how the low-mass stars could form continuously over such a long period in an environment that is characterized by strong winds of massive stars and frequent supernova explosions, which would disperse the molecular cloud, the raw material for star formation.

It has to be kept in mind that these two studies were based on a sample of only 28 low-mass PMS stars, found by investigation of a ~ 5 square-degree area in Upper Sco. The total area subtended by the association is about 100 square-degrees. Since there are 66 B star members in this area, one would expect roughly 1500 low-mass ($M_\star < 2\,M_\odot$) members if we assume a Miller & Scalo (1979)[1] log-normal IMF. Thus, the W94 sample contains only a tiny fraction of all low-mass PMS stars, and may be affected by spatial selection effects. In order to draw more reliable conclusions about the low-mass stellar population in Upper Sco, a significantly larger sample of low-mass PMS stars, selected homogeneously from a much larger area, should be used.

In this paper, we do use a considerably larger sample of ~ 100 low-mass PMS stars. These have recently been found by optical follow-up observations of ROSAT All Sky Survey X-ray sources. We determine basic stellar parameters and construct a new HR diagram of the Upper Sco association. This allows us to derive interesting conclusions on the star formation history of the association and on the initial mass function.

2. Low-mass PMS stars in Upper Scorpius

2.1. Searches for low-mass PMS stars

In order to obtain a larger sample of low-mass PMS stars, two large scale surveys have been performed recently. The first study was conducted by Kunkel (1999, K99 hereafter), who observed the optical counterparts of more than 200 ROSAT All Sky Survey (RASS) X-ray sources in a ~ 60 square-degree area in Upper Scorpius and Upper Centaurus-Lupus. The northern ~ 24 square-degree subarea of the K99 region overlaps with the area we use here and contains 32 stars which have strong enough lithium lines to be classified as PMS objects according to the criteria discussed in Preibisch et al. (1998).

The other study was a spectroscopic survey for PMS stars in a 160 square-degree area by Preibisch et al. (1998, P98 hereafter). The aim of this survey was to obtain a spatially complete (but flux-limited) sample of PMS stars over the *full area* of the association. In order to cover the huge area completely, the observations were performed with the wide-field multi-object spectrograph FLAIR at the United Kingdom Schmidt Telescope (UKST). The boundaries of our area were defined by the region covered by 6 individual $6° \times 6°$ UKST survey fields (see Fig. 1). Our area covers the Upper Sco association nearly completely and excludes the ρ Oph star forming region

[1] In this paper, for simplicity we use the Miller & Scalo IMF which for low-mass stars is fortunately close to modern IMF determinations (e.g. Kroupa et al. 1993; Scalo 1998).

at the eastern edge. Among the 78 observed X-ray selected candidates stars in the magnitude range $10.5 \leq B \leq 14.5$, P98 were able to identify 39 new PMS stars by their strong lithium lines.

A number of further searches have been performed, all of which, however, were focused on very small sub-regions of the association. For example, Meyer et al. (1993) studied IRAS sources in a ~ 2 square degree field near σ Sco and found 4 young stars. Sciortino et al. (1998) used deep pointed ROSAT X-ray observations to search for PMS stars in a ~ 4 square degree area near the center of our region and found several candidates for PMS stars. Martin et al. (1998) used pointed ROSAT observations in the vicinity of the ρ Oph star forming region. They found a number of additional PMS stars in our area, however all their new PMS objects which were not already detected by P98 or W94 are late K- or M-type stars, fainter than the magnitude limit of the P98 survey [2].

We also have performed a search for Hα emitting stars in Upper Sco. Using the ESO Schmidt telescope with an objective prism centered at Hα, one plate was obtained for a $5.4° \times 5.4°$ field centered at $\alpha = 16^{\rm h}\,06^{\rm m}$, $\delta = -21°$. A visual inspection of the plate did not show a significant number of Hα emitting objects. This is consistent with the very small number of Hα emitting classical T Tauri stars in Upper Sco listed in the Herbig-Bell Catalogue (Herbig & Bell 1988). In our 160 square-degree area, only the four CTTS HBC 602, AS 205 and AS 205/c, and HBC 256 are listed.

2.2. Definition of our PMS star sample

The sample of PMS stars we use in this paper consists of the PMS stars detected by P98 and those PMS stars from W94 and K99 which are located in our 160 square-degree field and which satisfy the lithium criterion used by P98. Since our aim was to get a spatially unbiased and homogeneous sample of PMS stars, we did not include the PMS stars detected only in the deep pointed ROSAT X-ray observations by Sciortino et al. (1998) and Martin et al. (1998).

All PMS stars in our sample are the counterparts of X-ray sources detected either in the RASS or in the EINSTEIN observations analyzed by W94, both of which have similar X-ray flux limits corresponding to $\log L_{\rm X}[{\rm erg/sec}] \gtrsim 29.8$. While W94 and K99 observed all X-ray sources in their fields, P98 used criteria based on the X-ray properties to select candidates for PMS stars among the numerous RASS sources in the field (see Sterzik et al. 1995 for details).

Our sample contains 95 PMS stars, 24 from W94, 32 from K99, and 39 from P98. It is spatially unbiased for X-ray sources with optical magnitudes in the range $10.5 \lesssim B \lesssim 14.5$. Of the 177 X-ray sources with optical counterparts in this magnitude range, 115 have been observed by W94, K99, or P98. This means that 65% of all X-ray selected stars in this magnitude range have been investigated. Although the sub-samples from W94 and K99 contain some optically fainter stars, most of the PMS stars fainter than $B \approx 14.5$ are systematically missing from our sample.

3. Spatial structure of the association

Since our sample is spatially unbiased, we can investigate the spatial distribution of the stars. There are two interesting aspects in this context: the spatial relationship between the low-mass PMS stars and the high-mass stars, and the line-of-sight depth of the association, which is very important for a proper interpretation of the HR diagram.

3.1. Projected spatial distribution

We made use of a list of all Hipparcos members in Upper Sco from de Zeeuw et al. (1999). The locations of the 87 Hipparcos members in our area are shown in Fig. 1 together with those of our low-mass PMS stars. Both samples show a similar, more or less homogeneous distribution within a roughly circular area with a radius of some 6° near the center of our field. At the mean distance of 145 pc, 6° correspond to a radius of about 15 pc.

3.2. Line-of-sight depth of the association

Although parallaxes are available for the Hipparcos members, the depth of their distribution along the

[2] There is one notable exception: According to Martin et al. (1998), the counterpart of the ROSAT source RXJ1614.2-1938 is a K2 PMS star. However, a closer inspection reveals only confusion: First, no stellar object with $B < 14.5$ is visible in the DSS image within 30″ of the optical position $\alpha(2000) = 16^{\rm h}\,14^{\rm m}\,15^{\rm s}$, $\delta(2000) = -19°\,38'\,40''$ given by Martin et al. Second, our own analysis of this ROSAT pointing does not confirm the X-ray source position given by Martin et al., but shows the source to be at $\alpha_{2000} = 16^{\rm h}\,14^{\rm m}\,11^{\rm s}$, $\delta_{2000} = -19°\,39'\,14''$. There are 5 rather bright ($B < 14$) stars in the vicinity of these positions. It is not clear which of these objects might be the K2 PMS star.

line-of-sight cannot be directly determined, because the parallax errors of ~ 1 mas do not allow to resolve the internal distribution of parallaxes (de Zeeuw et al. 1999). The standard deviation found for the Hipparcos parallaxes of the B and A star members is 1.3 mas. As noted by de Zeeuw et al. (1999), the spread in the observed parallaxes is fully consistent with the assumption of a spherical shape for the association, i.e. a line-of-sight depth of ~ 30 pc.

The scenario presented by Martin (1998), however, would require a very large depth of $\gtrsim 100$ pc. In that case, one would expect to find a broad distribution of parallaxes with a width of more than 7 mas. This is in sharp contrast to the very narrow distributions of parallaxes found for the Hipparcos members. We thus can exclude that the Hipparcos members have such a wide distribution along the line-of-sight. Since the projected distribution of the low-mass PMS stars is so similar to those of the Hipparcos members, it would be very hard to imagine how the PMS star spatial distribution could have a much larger depth than that of the Hipparcos members. We therefore conclude that the scenario proposed by Martin (1998) does not seem to be realistic.

4. Optical data for the PMS stars

For the PMS stars from W94 and K99 we use the spectral types, magnitudes and colors as reported in these studies. For the PMS stars from P98, magnitudes and colors have been determined as described next.

4.1. Photometric data

Our aim was to obtain photometric data for as many as possible stars in Upper Sco in order to see whether photometric selection criteria can be used to search for additional members of the association, especially among the fainter stars, for which the RASS selected sample is very incomplete. We thus decided to derive the photometry from the UKST Schmidt plates. The R and I plates for the UKST survey fields 584, 515, and 516 were measured for us with SuperCOSMOS, the Royal Observatory Edinburgh's advanced photographic plate digitizing machine (see Hambly et al. 1998). These three UKST survey fields cover the central ~ 100 square-degrees of our area, in which all but 6 of our PMS stars are located. SuperCOSMOS digitizes the photographic material to 15 bits with a resolution of 10 μm ($= 0.7''$). After scanning, the data are processed to detect astronomical objects. In each of our plates, between 6×10^5 and 1.2×10^6 objects were found, and for all these objects their positions, celestial coordinates, instrumental magnitudes and other parameters were determined. These data were finally supplied to us.

In order to calibrate the instrumental magnitudes, we determined the COSMOS magnitudes of the W94 PMS stars. Separately for each plate, we determined the relationship between the COSMOS magnitudes and the photoelectric magnitudes given by W94. We applied the color corrections given in Hambly (1998), i.e. transformed the photoelectric magnitudes into the "natural" system for the photographic data, and found that the data can be described quite well by relationships of the form $I = a + b \times I_{\rm COSMOS}$ and $(R-I) = c + d \times (R_{\rm COSMOS} - I_{\rm COSMOS})$. The use of more complicated relations did not improve the quality of the fit. This is probably due to the rather small range of colors ($R - I \sim 0.5 \ldots 1.5$) and magnitudes ($I \sim 9 \ldots 13$) covered by our stars. For each plate, we determined the coefficients a, b, c, and d, which subsequently were used to transform the COSMOS magnitudes of all objects on the plate to the standard photometric system. In Figure 2 we compare the calibrated COSMOS magnitudes and colors for the W94 stars to their standard photometric magnitudes and colors. The standard deviation is 0.16 mag for I, and 0.10 mag for $R - I$. This scatter is close to the expected accuracy of the COSMOS magnitudes (cf. Hambly 1998). We could identify 31 of the 39 PMS stars from P98 in the COSMOS data; for these stars we use the calibrated COSMOS photometric data.

4.2. The Color-Magnitude Diagram

In Fig. 3 we show the color-magnitude diagram for our PMS star sample. One can see that all objects, which were classified as PMS stars spectroscopically by their lithium lines, clearly lie well above the main sequence, confirming their PMS status. Furthermore, the stars populate a well defined locus in the diagram, with only very few outliers.

4.3. Determination of stellar parameters

In order to place the PMS stars into the HR diagram, we have to determine the extinctions, luminosities, and temperatures of the stars. For this, we have to take into account the PMS nature of the stars.

Since the relation between spectral type and effective temperature depends on surface gravity, the temperature scale for PMS stars is not identical to that for the main sequence stars. Several studies have found that most K and M type PMS stars show standard dwarf (luminosity class V) properties, while most G type and early K type PMS stars seem to be more similar to subgiant (luminosity class IV) stars (e.g. Herbig 1977; W94; Alcalá 1998). We thus used the tabulations of temperature as a function of spectral type and luminosity class of de Jager & Nieuwenhuijzen (1987) and constructed a temperature scale which corresponds to luminosity class IV for G type stars and to luminosity class V for K5 to M type stars, with a smooth transition in between.

We determined the extinction from the $R-I$ colors of the stars. The intrinsic colors were determined using the compilation of color as a function of stellar temperature given by Hartigan et al. (1994). Then, we computed the extinction from $A_V = 4.74\,E(R-I)$ (cf. Herbig 1998) and dereddened the I magnitudes, assuming $A_I = 0.482\,A_V$ (cf. Rieke & Lebofsky 1985). The extinctions we find are generally quite small ($A_V \lesssim 2$ mag) and do not show any systematic spatial variation in our field.

The bolometric luminosities of the PMS stars were computed from the dereddened I magnitudes, using the bolometric correction BC_I as a function of stellar temperature as given by Hartigan et al. (1994) and assuming a distance of 145 pc. The results are summarized in Table 1.

5. X-ray properties of the PMS stars

5.1. X-ray luminosities

The data we now have determined for the PMS stars allow us to compute their X-ray luminosities $L_{\rm X}$ and fractional X-ray luminosities $L_{\rm X}/L_{\rm bol}$. The transformation factor between the observed ROSAT count rate and the X-ray luminosity depends on the plasma temperature and the column density of X-ray absorbing material along the line-of-sight. We use the emissivities for the Raymond & Smith (1977) model of optically thin thermal plasma emission as implemented in EXSAS. Due to the low exposure times of the RASS data, the number of counts detected per source is too low for reasonable spectral fitting, which would allow to measure the plasma temperature. We thus assume a plasma temperature of $kT = 1$ keV, which is typical for PMS stars (e.g. Montmerle 1996; Preibisch et al. 1996) and also is consistent with the observed X-ray hardness ratios of these stars. For the computation of X-ray extinction we use the relation $N_{\rm H} = A_V \times 1.8 \times 10^{21}\,{\rm cm}^{-2}$ (Paresce 1984; see also Predehl & Schmitt 1995) in combination with the soft X-ray opacities of Morrison & McCammon (1983) as implemented in EXSAS. Using these parameters, we computed the transformation factor between the count rate and the *de*reddened X-ray flux with the corresponding EXSAS commands.

In Fig. 4 we plot the resulting fractional X-ray luminosities of the PMS stars as a function of bolometric luminosity. For comparison, we also have included data for the T Tauri stars in the Orion Nebula from Gagné et al. (1995). We note that the PMS stars in Upper Sco have X-ray properties very similar to those of PMS stars in other star forming regions. Nearly all stars show $\log{(L_{\rm X}/L_{\rm bol})} > -3.5$. The stars with the highest fractional X-ray luminosities were probably flaring during the RASS observations. This presumption can be checked using the results of Neuhäuser & Preibisch (1995), who analyzed the flares detected in the RASS observations of the Taurus Auriga star forming region, which is about at the same distance as Upper Sco. They found that the typical rate of RASS detectable flares per PMS star is about 1 flare every 40 days. Since the patrol time of the RASS observations in Upper Sco, i.e. the total elapsed time from the start of the first observation segment to the end of the last observation segment, is about 40 hours, one would expect that about 4%, i.e. some $3-4$ of the PMS stars in Upper Sco should have shown a flare during the RASS observations. This estimate suggests that the observed number of Upper Sco PMS stars showing exceptionally high fractional X-ray luminosities is fully consistent with PMS flare statistics.

5.2. Efficiency of the X-ray selection criteria for PMS stars

As noted above, W94 and K99 have investigated all optical counterparts of the X-ray sources in their fields, while P98 only obtained spectroscopy for those X-ray sources which had been classified as "PMS candidates" by their X-ray properties (see Sterzik et al. 1995 for details of the selection method). This selection method allowed P98 to reduce the sample of 606 RASS X-ray sources in our field to 180 PMS candidates and was the only way to make an efficient search for PMS stars feasible. However, it is also clear that this selection method will classify some of the unknown true PMS stars wrongly as non-candidates. We can use the PMS star samples from W94 and K99 to determine what fraction of RASS detected PMS stars would have been classified as non-PMS candidates, if the selection criteria would have been used. There are 39 RASS sources among the PMS stars of W94 and K99, and the X-ray selection method would have classified 33 of these sources correctly as PMS candidates. The other 6 of these stars would have been incorrectly classified as non-PMS candidates, e.g. because their X-ray/optical flux ratio or their X-ray colors are not in the typical range for PMS stars. This means that we can expect this X-ray selection method to classify a fraction of $6/39 = (15 \pm 6)\%$ of the PMS stars wrongly as non-PMS candidates. For any RASS detected PMS star, the probability for being correctly classified as a PMS candidate is 85%, i.e. this selection works quite well.

6. Contamination by young foreground stars ?

It is well known that the decay of lithium in young G-type stars is much slower than in K- and M-type stars (e.g. D'Antona & Mazzitelli 1994). Some $10 - 100$ Myr old G-type stars show only slightly weaker lithium lines than G-type PMS stars with ages of a few Myr. Since these older, but still young, stars can show similar levels of X-ray activity as the very young PMS stars, one is in danger to contaminate the PMS sample in a star forming region by young foreground stars. If unrecognized foreground stars are placed into the HR diagram, erroneously assigning to them the same distance as to the PMS stars in the star forming region, their luminosities will be overestimated and thus their isochronal ages will be underestimated, making them mimic much younger PMS stars.

Indeed, the samples of RASS X-ray selected PMS stars in several star forming regions, which suggested a very wide spatial distribution of PMS stars around these regions (e.g. Alcalá et al. 1996; Krautter et al. 1997), have later been found to be contaminated by young foreground stars (e.g Alcalá et al. 1998; Wichmann et al. 1997). A detailed investigation of this widely scattered population of lithium rich and X-ray active stars has shown that most of these objects are not associated to the corresponding star forming regions, but to a population of young foreground stars. These foreground stars seem to be related to the Gould Belt, a large ring-like galactic structure containing young stars with typical ages of $\sim 40 - 80$ Myr (cf. Guillout et al. 1998).

In this study, we have been aware of this problem and thus have tried to avoid a contamination by young foreground stars as far as possible. We are confident that our sample of PMS stars is not significantly contaminated for the following reasons:

One of the problems in the older studies yielding contaminated samples was the use of insufficient spectral resolution, that caused the equivalent with of the lithium line, $W(\mathrm{Li})$, to be overestimated. All stars in our sample have been observed at high enough resolution to avoid such problems (cf. discussion in P98). Another problem in the older studies was the use of too low lithium equivalent width limits for the classification of PMS stars. For example, Alcalá et al. (1996) and Krautter et al. (1997) originally classified all stars with $W(\mathrm{Li}) > 0.1$ Å as PMS stars. For our sample of PMS stars we have used a much stricter and spectral type dependent line width criterium which is described in detail in P98. Our lithium criterium requires minimum equivalent widths between 0.2 Å and 0.35 Å and makes sure that only stars with $W(\mathrm{Li})$ exceeding the maximum $W(\mathrm{Li})$ for $\gtrsim 30$ Myr old cluster stars are classified as PMS stars.

The young foreground stars among the PMS candidates of the earlier studies typically show lithium equivalent widths close to or below the maximum found for Pleiades stars (cf. Alcalá 1998). Since the lithium equivalent width of nearly all our PMS stars exceeds the maximum equivalent width for Pleiades stars by at least 0.1 Å, we can be confident to have excluded most young foreground stars.

Furthermore, we also have kinematic evidence for most of our PMS stars that they actually are members of the Upper Sco association: All stars in the subsample of W94 with known radial velocities are radial velocity members of the association, and all our PMS stars for which proper motion data are available, show proper motions consistent with kinematic membership to the association (see discussion in P98).

Thus we conclude that any contamination of our PMS star sample with young foreground stars is very small if present at all.

7. The HR diagram

In order to derive stellar ages and masses from the HR diagram, we use the PMS evolutionary tracks of D'Antona & Mazzitelli (1994; DM94). These tracks have the advantage that they are well tested and successfully reproduce the empirical isochrones for young clusters (e.g. Stauffer et al. 1995). Furthermore, they are widely used and thus allow a direct and consistent comparison of our results with the findings of other studies. Stauffer et al. (1995) have shown that for stars later than M1, the use of the standard dwarf temperature scale of Bessell (1979) gives implausible results in combination with the DM94 tracks, causing the ages and masses of the M stars to be systematically underestimated. They also demonstrated that this inconsistency can be avoided if the M star temperature scale of Kirkpatrick et al. (1993) is used. Since the de Jager & Nieuwenhuijzen (1987) dwarf temperature scale is similar to the Bessell (1979) scale, we adopted the temperature scale of Kirkpatrick et al. (1993) for the M2 and M3 stars in our sample. Fig. 5 shows our HR diagram. It contains 86 PMS stars. Before we derive any conclusions from the HR diagram, a careful discussion of the completeness of our sample is necessary.

7.1. Completeness

Our sample of PMS stars is spatially unbiased for all X-ray detected objects in the magnitude range $10.5 \leq B \leq 14.5$. The selection effects can be characterized in the following way.

7.1.1. X-ray completeness

All our PMS stars were selected from X-ray observations with a flux limit corresponding to a limiting X-ray luminosity of $\log L_{\rm X}[\mathrm{erg/sec}] \gtrsim 29.8$ at the distance of Upper Sco. It is not possible to determine the X-ray completeness, since this would require knowledge of the X-ray luminosity function of these stars. Unfortunately, the X-ray luminosity function of PMS stars is not well known, because all samples of PMS stars investigated so far, are more or less strongly biased for X-ray selected objects. Thus, one cannot exclude the possible existence of a population of PMS stars which have X-ray luminosities much lower than typical for the known PMS stars.

For late type stars, X-ray luminosity is correlated to the bolometric luminosity (cf. Montmerle 1996, Preibisch et al. 1996), and the ratio $L_{\rm X}/L_{\rm bol}$ is a good indicator for PMS stars. From figure 4 one can see that all PMS stars in our sample show $\log(L_{\rm X}/L_{\rm bol}) \gtrsim -3.5$. Thus, we have to expect that our X-ray selected sample is incomplete for stars with $\log(L_{\rm X}/L_{\rm bol}) \lesssim -3.5$. This limit can be easily transformed into a limiting bolometric luminosity, yielding $\log(L_{\rm bol}/L_{\odot}) \approx -0.33$. By comparison with the PMS tracks in the HR diagram one can see that stars with $M \geq 1\,M_{\odot}$ should be detectable at any age, if their fractional X-ray luminosity is $\log(L_{\rm X}/L_{\rm bol}) \geq -3.5$. Less massive M-type PMS stars with the same fractional X-ray luminosity, however, would only be detectable if they are very young ($\lesssim 1$ Myr). We thus conclude that our X-ray selected sample is probably significantly incomplete for stars with masses of $< 1\,M_{\odot}$.

Direct evidence for this X-ray incompleteness comes from the observations of Martin et al. (1998) and Sciortino et al. (1998): several late K- and M-type PMS stars were found among the optical counterparts of faint X-ray sources, which were detected in deep pointed ROSAT X-ray observations, but not in the RASS.

7.1.2. Optical completeness

Another selection effect comes from the magnitude limit ($B \leq 14.5$) used in the target selection process for the FLAIR observations. We have transformed this magnitude limit into the corresponding luminosity limit, using the $B-V$ colors and BC_V from Hartigan et al. (1994). The limiting luminosity is indicated in Fig. 5. Above this limit, the optical completeness of our sample is equal to the fraction of observed X-ray sources in this magnitude range, i.e. 65%. The numerous M-stars which lie considerably below this limit are from the sub-samples of W94 and K99, which contain also fainter stars.

Taking optical and X-ray completeness together, we conclude that our sample is spatially unbiased for stars with masses $\gtrsim 1\,M_{\odot}$. Our sample is definitely incomplete for M-type stars, where we have a strong selection effect for luminous, i.e. young PMS objects. We note that the upper magnitude limit ($B \geq 10.5$) of the FLAIR observations might introduce some incompleteness for stars with masses above $\sim 1.7\,M_{\odot}$.

7.2. Interpretation of the HR diagram

The usual way to interpret the HR diagram is to derive the mass and age of each star from its location in the diagram. We did this and list the derived ages and masses for our PMS stars in Table 1. However, there are (at least) two problems associated with these ages and masses which make the interpretation difficult. The first problem is that the ages derived in this way will systematically underestimate the true ages because of the presence of unresolved binary systems. We thus will denote the ages derived from the position in the HR diagram as "isochronal ages" in order to discern them from the true stellar ages. The second problem is that the errors in the masses and ages strongly depend on the position of the star in the HR diagram. For example, if we overestimate the luminosity of an M0 star by a factor of 2 due to an unresolved companion, we will underestimate the age of this stars by about a factor of 4. For a G5 star, however, the same error in luminosity will only produce an underestimate of the age by about a factor of 2. This effect makes it very difficult to interpret the spread in the isochronal ages. We thus decided to use a different approach, which is described in the next subsection.

7.3. Modeling the HR diagram

Our modeling procedure works as follows: We specify a model for the star formation history, and then determine the expected locations of the stars in the HR diagram, taking proper account of possible errors. Finally, a comparison of the locations of the stars with the expected region in the HR diagram shows whether the model is consistent with the data or not. For this modeling we will only consider errors in the stellar luminosities, since the luminosity errors cause much larger uncertainties for the stellar ages than the errors in stellar temperature.

Our model for the star formation history assumes that all stars have the same age. If there were no errors, all stars should lie on the corresponding isochrone. A spread of individual stellar distances, photometric errors, and the presence of unresolved binaries, however, will cause deviations, and widen the isochrone to a band. The modeling of photometric and distance errors is straightforward. The errors caused by unresolved binaries, however, are more complicated and require detailed modeling.

7.3.1. Modeling the effect of unresolved binaries

We have performed extensive simulations of binary systems to investigate their effects on the stellar positions in the HR diagram. We assume that the measured spectral type of an unresolved binary always is that of the primary, since the primary will dominate the combined spectrum. An unresolved companion causes an overestimate of the stellar luminosity in two different ways. The first and obvious effect is that the flux we measure corresponds to the system luminosity and not to the primary luminosity. The second effect is that the companion also causes an color excess, i.e. the $R-I$ color of the binary system is redder than the $R-I$ color of the primary star. This causes the extinction to be overestimated and also leads to overestimate the luminosity (cf. Brandner & Zinnecker 1997).

Since these two effects strongly depend of the masses of the primary and the companion, we have simulated large numbers of artificial binary systems. The basis of our simulations is the result of Duquennoy & Mayor (1991) that the binaries in the field can be explained by random pairing of stars from the same IMF (see also Malkov et al. 1998). For any primary, we randomly draw 30 000 companion masses from a Miller & Scalo (1979) IMF, i.e. using a probability distribution with density[3]

$$\frac{\mathrm{d}N}{\mathrm{d}M} \propto \begin{cases} M^{-1.4} & \text{for} \quad 0.1 < M/M_\odot < 1 \\ M^{-2.5} & \text{for} \quad 1 < M/M_\odot < 10 \end{cases}$$

with the restriction that the companion mass must not exceed the primary mass. We then use the PMS evolutionary tracks of DM94 for the age of 5 Myr to determine the luminosity and temperature of each star according to its mass. This allows us to compute the system luminosity and the factor by which the luminosity of the primary is overestimated due to the presence of the companion. Then, the $R-I$ colors of the stars are determined from a fit to the tabulation of $R-I$ and $T_{\rm eff}$ given by Hartigan et al. (1994). Similarly, BC_I is determined as a function of $T_{\rm eff}$. This allows us to compute the $R-I$ color for the system. A comparison with the $R-I$ color of the primary then yields the factors by which the extinction and the system luminosity are overestimated due the red excess caused by the companion. Taking everything together, this finally yields the factor $\Delta \log L$ by which the luminosity of the primary is overestimated for each simulated system. We performed these simulations for a range of different primary masses. For each primary mass, we have computed the mean, the 90% quartile, and maximum of $\Delta \log L$. These results are summarized in Table 2.

[3]This formula is consistent with recent IMF determinations (cf. Scalo 1998); small changes of the exponents do not alter our modeling results noticeably.

7.3.2. *Result of the modeling*

The expected locations in the HR diagram can now be determined in the following way: We assume photometric errors of $\Delta I = 0.16$ mag, $\Delta(R-I) = 0.1$ mag, and an uncertainty of about one subclass in the spectral types. This causes an luminosity error of $\Delta \log L = 0.12$. If we also include the errors caused by a spread of distances of $\Delta d = \pm 15$ pc, we find $\Delta \log L = 0.15$. If we assume the errors to be normally distributed, then the 90% confidence error band is given by $\Delta \log L \sim \pm 0.25$. To this, we add the 90% quartile of the luminosity overestimation factors as a function of primary mass as determined above. The final error band is shown as the grey shaded area in Fig. 5. The expectation that 90% of the PMS stars should lie within this band, is very well confirmed, since only 9 of our 86 PMS stars lie outside the band. *This means that the HR diagram is consistent with the conclusion that all PMS stars have an age of 5 Myr.*

We also have checked how well the data are consistent with other model ages. If we increase the model age slightly, the agreement between model and data gets worse very quickly: for a model age of 7 Myr, the number of stars lying outside the error band is 20, indicating that the observational data and the model are no longer consistent. If we decrease the model age to 3 Myr, the error band no longer reproduces the general shape of the distribution of the G- and K-type PMS stars. We conclude that the model is consistent with the data only in a quite narrow range of assumed ages, about $4-6$ Myr.

8. Interpretation

8.1. Stellar ages

8.1.1. *The mean age*

The mean age of the PMS stars can be determined from the isochronal ages, if we take into account the completeness limits and the effects caused by unresolved binaries. First, we will consider only the stars with $M_\star \geq 1\,M_\odot$, for which our sample is unbiased. For the mean and the central 68% quartile of the isochronal ages of these stars we find $\langle\tau_{\rm iso}\rangle = 4.5^{+3.5}_{-2.7}$ Myr. The spread of isochronal ages is rather large, because it includes all uncertainties, i.e. photometric errors, the distance spread, and binarity effects. The spread of the true ages must therefore be considerably smaller (see next paragraph).

In order to transform this value into an estimate of the mean true age, we use the results in Table 2 to take into account the effect of unresolved binaries. For the range of masses considered here, the average luminosity error caused by unresolved binaries is $\langle\Delta \log L\rangle \approx 0.1$. Brandner & Köhler (1998) have presented K-band speckle data for 56 of the PMS stars in our sample. They found that about half of the $M_\star \geq 1\,M_\odot$ PMS stars are binaries which are unresolved in our data (i.e. with separations $< 3''$). Thus, the correction factor we have to apply is $\langle\Delta \log L\rangle \approx 0.05$, and this implies that the mean of the true ages should be about a factor of 1.2 higher than the mean of the isochronal ages. This yields $\langle\tau\rangle \approx 5.4$ Myr, and is in very good agreement with the age of $(5-6)$ Myr found for the B stars.

We can also consider the stars with lower masses. Since our sample contains only the brightest stars with masses below $1\,M_\odot$, it is clear that we can only derive a lower limit for the true mean age. The mean of the isochronal ages for the stars with $M_\star \leq 0.45\,M_\odot$ is $\langle\tau_{\rm iso}\rangle = 1.3^{+1.5}_{-0.8}$ Myr. As noted by Brandner & Köhler (1998), almost all of the brighter M-type PMS stars in Upper Sco are binaries. This is most likely a consequence of the fact that binaries are optically brighter and also have higher X-ray luminosities than single stars. Any X-ray selected and magnitude limited sample of PMS stars thus will preferentially contain binaries. Thus, we here assume a binary fraction of 100%. Then, the luminosity correction factor is $\langle\Delta \log L\rangle \approx 0.31$. This implies that the lower limit for the true ages should be about a factor of 3.2 higher than the isochronal ages, yielding $\langle\tau\rangle > 4.3$ Myr. Even if we assumed a more conservative binary fraction of only 80% for these stars, we would find $\langle\tau\rangle > 3.3$ Myr. These lower limits agree well with the above result for the more massive stars.

Taking everything together, the mean age of the PMS stars seems to agree very well with the range of $(5-6)$ Myr found for the B stars.

8.1.2. *Age spread*

It is not easy to disentangle a possible age spread from the scatter caused in the isochronal ages by observational errors. The standard deviation expected from photometric and distance errors as estimated above should cause luminosity errors of $\Delta \log L = 0.14$. Including the uncertainties in the stellar temperatures of $\Delta \log T \sim 0.015$ and the effects of unresolved binaries as discussed above, the expected spread of isochronal ages due to these errors should be $\Delta \log \tau_{\rm iso} \sim 0.30$. The central 68% quartile of the logarithmic ages of the $M_\star \geq 1\,M_\odot$ stars has a half-width of $\Delta \log \tau_{\rm iso} = 0.33$. Since this is just the scatter expected from the errors, we conclude that our data provide no evidence for a significant spread of ages. A small age spread cannot be excluded, but is probably not larger than about 2 Myr.

8.1.3. Comparison with the ages derived by W94

How can we explain the significantly younger ages derived by W94? The first point is that W94 assumed a distance of 160 pc instead of the 145 pc we use here. This decrease of distances and the corresponding decrease of luminosities causes the isochronal ages to increase by about a factor of 1.4. This raises the W94 age estimate from $\sim$ 1.2 Myr to $\sim$ 1.7 Myr. The mean of the isochronal ages we find here for the W94 stars is $\sim$ 2.0 Myr. The slight, but insignificant difference can be understood by the different ways in which stellar luminosities were determined from the photometric data.

If only the stars with $M_\star \geq 1\,M_\odot$ are considered, then we find a mean age of (3.3 ± 2.6) Myr for the W94 sample. For the stars from K99 and P98 in that mass range, we find (4.9 ± 4.3) Myr. Although the difference is not significant, it indicates that the sample of W94 might not be representative for the full population of PMS stars in Upper Sco. This might perhaps be related to the small area from which the W94 stars were selected: all but two of the W94 PMS stars were selected from a $\sim$ 3 square-degree subregion.

8.1.4. Comparison with the ages derived by Martin (1998)

Our result of a small age spread is in a notable contrast to the large spread of ages ($1-20$ Myr) suggested by Martin (1998; M98 hereafter) from the analysis of the lithium line widths of the PMS stars from W94. We see several problems with the interpretation of the lithium data by M98, which can explain this difference.

The first problem is that M98 assumes an average distance of only 125 pc for Upper Sco, computed as the mean distance of only four B stars. Since the mean distance determined from the much larger sample of all 178 Hipparcos members by de Zeeuw et al. (1999) is (145 ± 2) pc, M98 clearly underestimated the true mean distance, and thus overestimated the stellar ages.

The second point is related to M98's method to estimate stellar ages from the lithium line widths. His argument for the presence of a large age spread is not based on individual stellar ages, but on his classification of about half of the stars as "post T Tauri stars", for which typical ages of $10-20$ Myr are assumed, and the other half as T Tauri stars with typical ages of a few Myr. We do not believe that the observed lithium line widths provide evidence for a significant age spread for the following reasons: For G and early K stars, lithium depletion is not only a function of age, but also depends strongly on other factors such as stellar rotation (cf. Soderblom 1996). Therefore, the spread of lithium line widths for these stars is not a good argument for a large age spread. The late K and the M stars are known to deplete their lithium very quickly (e.g. D'Antona & Mazzitelli 1994; Bildsten 1997), because they are fully convective. The mean value and standard deviation of the lithium line widths of these stars in our sample is (0.5 ± 0.1) Å. According to the curves of growth from Pavlenko & Magazzu (1996) this scatter corresponds to a spread of lithium abundances of about 1 dex, and theoretical models of lithium depletion show that this implies an age spread of not more than $\sim$ 20% (Bildsten 1997). We thus conclude that the observed spread of lithium line widths does not necessarily imply a large spread of ages as claimed by Martin (1998).

Furthermore, we note that Martin's classification scheme does not seem to be well founded for the late K and M stars. The dividing line between T Tauri stars and "post T Tauri stars" in this spectral range is not based on physical arguments but given by a constant extrapolation of the minimum line width for K7 stars. Since all but two of the Upper Sco stars classified as "post T Tauri stars" by Martin (1998) are in this spectral range, this classification does not seem to be very reliable.

8.1.5. Spatial distributions of stellar ages

In Fig. 6 we show the IRAS 100 μm map of the region on which we have overplotted the positions of the PMS stars with symbol size marking the isochronal age of the stars. One cannot see any systematic spatial age gradient.

It is interesting to note that the radial velocity dispersion measured for the PMS stars of W94 is 1.8 km/sec. In a period of $\sim (5-6)$ Myr this corresponds to a linear distance of about 10 pc. This agrees very well with the projected radius of the association of about $10-15$ pc (see Section 3) and indicates that the stars might have been in a considerably denser configuration at the time of their formation. It seems possible that the association started as a relatively compact cluster which then expanded because it became gravitationally unbound (cf. Elmegreen et al. 1999).

8.1.6. On the fraction of classical T Tauri stars

Our sample of 98 PMS stars contains only 4 CTTS (defined by $W(\mathrm{H}\alpha) \geq 10$ Å). As already noted by W94, the fraction of CTTS in Upper Sco is much lower than typically found for regions with ongoing star formation. For example, in the ρ Oph cloud the fraction of CTTS among the PMS stars is about 50%. We believe that the low fraction of CTTS in Upper Sco is the consequence of the age of the stars and their environment. While the survival times of circumstellar disks around individual PMS stars can vary widely from $\lesssim 0.1$ Myr to $\gtrsim 10$ Myr, typical values seem to be a few Myr (see discussion in Bouvier et al. 1997). At an age of $3-5$ Myr, the typical fraction of stars with disks is about 30% – 50% in other star forming regions. The fraction of $< 10\%$ we find here for Upper Sco, seems to be significantly lower than this and indicates that the dissipation of circumstellar disks around the PMS stars in Upper Sco happened faster than in other star forming regions. It might well be that this is the consequence of the strong winds and ionizing radiation of the numerous luminous stars in Upper Sco, which have accelerated disk dissipation. Furthermore, the supernova which exploded in Upper Sco about 1.5 Myr ago, probably also contributed to this effect.

8.2. On the initial mass function (IMF) of the association

Upper Sco is a good place to study the IMF, because the star formation process is finished, i.e. the initial mass function is "ready", and all young stars are optically visible since the parental molecular cloud is nearly fully dispersed. W94 were the first to investigate the low-mass function of the Upper Sco association. They concluded that the initial mass function in the range $(0.3-2)\,M_\odot$ seems to be consistent with a Miller-Scalo field IMF within the uncertainties. However, this result is subject to substantial uncertainties due to low-number statistics (only 28 stars) and the use of large and very uncertain completeness corrections.

As compared to W94, we now have the advantage of a much larger sample of PMS stars and a much better spatial coverage of the association. Furthermore, the Hipparcos data resulted in a much better knowledge of the population of high-mass stars. However, due to our optical magnitude limit, the optical completeness of our sample is lower than that of the W94 study. We thus can derive firm conclusions on the IMF only for masses above $\sim 1\,M_\odot$. We will not try to construct an empirical initial mass function; here we will restrict ourselves to the determination of the ratios for the numbers of stars in different mass ranges, which can be compared to the ratios expected from theoretical initial mass functions.

8.2.1. Stellar masses from $1\,M_\odot$ to $1.5\,M_\odot$

As discussed above, we can assume our sample to be spatially unbiased and reasonably complete for stars in the mass range $1\,M_\odot \leq M_\star \leq 1.5\,M_\odot$. Our sample contains 21 PMS stars in this mass range. In our area there are 21 Hipparcos members with $M_\star \geq 3\,M_\odot$ (corresponding to a ZAMS spectral type of B8 according to Palla & Stahler 1993). Given this number of high-mass stars, one would expect to find

$$\begin{array}{ccccc} N(1-1.5) = N(>3) & \times & \dfrac{F(>1)-F(>1.5)}{F(>3)} & = & \\ 21 & \times & 1.9 & = & 40 \pm 6 \end{array}$$

PMS stars in the $(1-1.5)\,M_\odot$ mass range, where F denotes the fraction of stars in the corresponding mass range and is determined from Table 9 in Miller & Scalo (1979).

We have to correct the observed number of low-mass stars for optical and X-ray incompleteness. The correction for optical incompleteness is easy, since the completeness simply corresponds to the fraction of observed RASS sources, i.e. 65% (see Section 2.2). The difficult correction is that for the number of PMS stars which have X-ray luminosities below our detection threshold. It is very hard to obtain information about this, because most samples of PMS stars are heavily biased for X-ray selected stars, i.e. a population of "X-ray quiet" PMS stars would be very hard to find. Note that P98 performed a search for "X-ray quiet" PMS stars in Upper Sco by observing stars which were not detected as RASS X-ray sources, but were selected as possible association members by their proper motions. *Although more than 100 such "X-ray quiet" proper motion candidates were observed, none of these stars turned out to be a PMS object.* From this, P98 concluded that the X-ray selected sample of PMS stars must be at least 75% complete for stars in the magnitude interval $11.5 \lesssim B \lesssim 13.5$. Walter et al. (1997) reported the detection of a population of X-ray quiet PMS stars in the σ Orionis cluster. Among several hundred optically selected candidates with $V \lesssim 16.5$ they could find 104 PMS stars, 28 of which were not detected in deep ROSAT X-ray observations with a flux limit corresponding to about 2×10^{29} erg/sec. This means that the X-ray selected sample around σ Orionis is 73% complete. Compared to the P98 survey for X-ray quiet PMS stars the Walter et al. (1997) survey is about 5 times deeper in the optical and about 3 times deeper in X-rays; this explains why Walter et al. (1997) were able to find X-ray quiet PMS stars, whereas P98 could only derive an upper limit on the number of such stars. These results suggest a completeness of 75% to be a reasonable assumption for our sample of PMS stars in Upper Sco.

Applying now the corrections for optical completeness (65%) and X-ray completeness (75%), the corrected number of low-mass stars is $N(1-1.5) = 21/(0.65 \times 0.75) = 43$. This agrees with the expected number of 40 ± 6 within the uncertainties. We conclude that the number of low-mass PMS stars is in reasonable agreement with that expected from the Miller-Scalo field IMF.

8.2.2. Stellar masses below $1\,M_\odot$

Unfortunately, our sample does not allow us to study the mass function at lower masses. This would be very interesting because one might speculate that the physical conditions in the association could be unfavorable for the formation of low-mass stars (bimodal star formation). From the results above and the Miller-Scalo IMF one would expect ~ 700 stars with masses between $1\,M_\odot$ and $0.1\,M_\odot$ to be present in our field in Upper Sco. These stars, however, are very hard to find, since they are not only faint in the optical but also too faint in X-rays in order to be detected in the RASS. Some of these stars can be found among the fainter X-ray sources detected in deep X-ray observations (cf. Martin et al. 1998; Sciortino et al. 1998), but in order to include also X-ray quiet PMS stars, optical selection criteria should be used.

A possible way to find these stars would be to select candidates from a color-magnitude diagram (CMD). In Fig. 7 we show the CMD constructed from our SuperCOSMOS data for all 25 930 stars with $I < 16$ within a 12 square-degree sub-area at the center of our field. We have also included the known PMS stars into this plot, which can be seen to populate a well defined band in the CMD. This band contains some ~ 380 additional stars, which are good candidates for PMS stars, although a significant fraction of them are probably field stars. This number can be compared to that expected from the number of high-mass stars in this sub-area, assuming again a Miller-Scalo IMF: it predicts ~ 170 stars with masses of $(0.1-1)\,M_\odot$. From this comparison one can see that there seems to be no evidence for a deficit of low-mass stars. Any further conclusions would require a large spectroscopic survey for fainter PMS stars.

8.3. On the star formation rate

Since we have found that the number of low-mass PMS stars seems to be consistent with the field IMF, we assume the total mass of all stars in Upper Sco to be $\sim 2350\,M_\odot$, as derived by de Geus (1992) by extrapolation of the field IMF to low masses. If all these stars have formed within a period of ~ 2 Myr, the star formation rate would have been $\psi \approx 1 \times 10^{-3}\,M_\odot$/yr. This number can be compared to other star forming regions. For extended T associations, star formation rates between $\psi \approx 2.5 \times 10^{-5}\,M_\odot$/yr, as found for the Chamaeleon I cloud, and $\psi \approx 1 \times 10^{-4}\,M_\odot$/yr, as found for the Taurus-Auriga cloud, seem to be typical (see Feigelson 1996). Similar star formation rates of $\psi \approx 4 \times 10^{-5}\,M_\odot$/yr were derived for the young clusters IC 348 and NGC 1333 in the Perseus molecular cloud complex (Lada & Lada 1995; Lada et al. 1996). For the Orion Nebula cluster, the results of Hillenbrand & Hartmann (1998) suggest $\psi \approx 1 \times 10^{-3}\,M_\odot$/yr.

From these numbers one can see that the star formation rate of the Upper Sco association is at least about one order of magnitude larger than typical for T associations or loose young open clusters, but comparable to the high star formation rate in the dense Trapezium cluster. We interpret this as another indication that the formation of the stars in Upper Sco was triggered[4]. The star formation process in Upper

[4] Triggering compresses the pre-stellar gas causing a synchronized and rapid collapse of the gas, i.e. a shorter contraction and collapse time due to the induced higher gas density, hence

Sco thus can be considered as a burst of star formation during which the stars have been forming much faster than typical for the quiescent conditions in T associations, where the stars seem to form more continuously over time.

Interestingly, the ρ Oph star forming region seems to form stars at a rate quite comparable to Upper Sco: the cloud contains ≈ 2000 stars (Kenyon et al. 1998), and if we assume an average stellar mass of $\approx 0.5\,M_{\odot}$ and an age of ~ 1 Myr, we find $\psi \sim 1 \times 10^{-3}\,M_{\odot}/\mathrm{yr}$. This fits well because there is evidence that the star formation process in ρ Oph is triggered by the shock wave from the supernova explosion in Upper Sco (see below).

9. Conclusions

9.1. The star formation history of Upper Sco

To summarize the above results, we find that the low-mass PMS stars have ages of about 5 Myr, with a rather small dispersion. This agrees very well with the age of the massive stars and indicates that high-mass and low-mass stars have formed more or less simultaneously. There are two main implications we derive from these results.

The first implication is that our results strongly suggest that *the star formation process in Upper Sco was triggered*. Interestingly, a suitable trigger seems to be available: As discussed by de Geus (1992), the Scorpius-Centaurus association is surrounded by several large H I loops, which were created by supernova explosions and stellar winds. The largest and thus oldest of these shells is centered on the Upper Centaurus-Lupus association, which is the oldest subgroup of Scorpius-Centaurus. The kinematic properties of this shell ($v \sim 10$ km/sec, radius ~ 110 pc) suggest that the corresponding shock wave passed through the former Upper Sco cloud about 5 Myr ago. This time agrees very well with the stellar ages in Upper Sco. Such a slow shock wave of a relatively distant[5] supernova is precisely what is required to induce star formation by causing cloud cores to collapse (cf. Foster & Boss 1996). The supernova shock wave from Upper Centaurus-Lupus as a trigger for the star formation process in Upper Sco thus provides a self-consistent explanation for the data.

The second implication is that, after a short starburst, the star formation process must have been halted; otherwise one could not understand the small spread of ages found for the high-mass as well as for the low-mass stars. The most likely reason for this is the influence of the numerous massive stars, which formed simultaneously with the low-mass stars. The most massive stars reached the main sequence within a few 10^5 years after the beginning of the star formation process in Upper Sco, and their strong winds and ionizing radiation immediately started to disperse the molecular cloud. An upper limit for the mass of the original cloud is given by the mass of the HI shell surrounding Upper Sco, which is $\sim 80\,000\,M_{\odot}$ (de Geus 1992). The total amount of kinetic energy of the stellar winds in Upper Sco is $\sim 1.7 \times 10^{50}$ erg (de Geus 1992). With this amount of kinetic energy one can accelerate a cloud mass of $80\,000\,M_{\odot}$ to velocities of ~ 15 km/sec. This rough energy estimate shows that the stellar winds have been perfectly capable of dispersing the remnant gas and dust in the Upper Sco cloud within at most a few Myr after the onset of the star formation process.

About 1.5 Myr ago, the most massive star in Upper Sco (presumably an O7 star with $40\,M_{\odot}$; cf. de Geus 1992) exploded as a supernova. This explosion produced a shock wave with an kinetic energy of $\sim 10^{50}$ erg and possibly the runaway star ζ Oph (de Geus 1992). This shock wave fully dispersed the remnant cloud material in Upper Sco. The wave now expands with a velocity of ~ 10 km/sec (de Geus 1992) and must have reached the ρ Oph cloud within the last 1 Myr. Interestingly, the ρ Oph cloud actually shows evidence for compression from the rear south-western side and for the presence of a slow shock (cf. Motte et al. 1998). It seems that the same shock wave which fully destroyed the Upper Sco cloud now triggers star formation in ρ Oph. This might sound confusing, but is well consistent with recent theoretical results on the interaction between shock waves and clouds: according to the numerical simulations of Foster & Boss (1996), the impact of a shock wave on a cloud core strongly depends on the nature of the shock. The initial, adiabatic phase of a shock wave is likely to destroy ambient clouds, while the later, isothermal phase is capable of triggering cloud collapse. Foster & Boss (1996) investigated an explosion with an initial kinetic energy of 2×10^{50} erg, which is similar to that of the Upper Sco supernova. For this model, they

an increased rate of star formation (in other words a mini-starburst).

[5]The distance from Upper Centaurus-Lupus to Upper Sco is about 70 pc.

find the switch between the adiabatic and isothermal phase to be at a radius of about 14 pc. This explains why such an explosion has dispersed the remnant cloud material in Upper Sco (radius ~ 12.5 pc), whereas the later stage of the wave now is able to instigate cloud collapse and trigger star formation in the ρ Oph cloud, which has a distance of about 20 pc from the center of Upper Sco.

9.2. The global picture: Star formation in the Scorpius-Centaurus OB association

We note that all the available results now fit very nicely into a general picture of the star formation history of the Scorpius-Centaurus association, which can be outlined as follows (see illustration in Fig. 8; see also de Geus 1992; W94): The star formation process in Scorpius-Centaurus started in the Upper Centaurus-Lupus association some 15 Myr ago. About 12 Myr ago the most massive star in Upper Centaurus-Lupus exploded as a supernova and created the largest of the H I shells surrounding the association. The shock wave from this supernova passed through the Upper Sco cloud about 5 Myr ago (A), triggering star formation there. Shortly thereafter, the strong winds of the numerous massive stars in Upper Sco started to disperse the molecular cloud and halted the star formation process (B). About 1.5 Myr ago the most massive star in Upper Sco exploded as a supernova (C). This shock wave fully dispersed the Upper Sco molecular cloud and now passes through the ρ Oph cloud, where it started the star formation process about 1 Myr ago (D) [A,B,C, and D refer to Fig. 8].

The spatial and temporal structure of the Scorpius-Centaurus OB association begs the question whether most stars in the association originally formed in a much denser configuration, i.e. a cluster which was unbound, or whether the stars were rather born in an already scattered assembly, similar to their current appearance (cf. Elmegreen et al. 1999). This question remains to be answered, perhaps with future astrometric missions.

We would like to thank Harvey MacGillivray and the SuperCOSMOS Group at the Royal Observatory Edinburgh for scanning the UKST plates for us. We are grateful to A. Brown for several very helpful comments on the manuscript and for communicating to us the results of the Hipparcos membership determinations before publication. Thanks are due to the referee (F.M. Walter) whose report was much appreciated. This work was supported by the DFG under grant Yo 5/18-1,2. TP acknowledges a fellowship of the Max-Planck-Society. The ROSAT project was supported by the Bundesministerium für Bildung, Wissenschaft, Forschung und Technologie (BMBF/DLR) and the Max-Planck-Society.

REFERENCES

Alcalá J.M., Terranegra L., Wichmann R., et al., 1996, A&AS 119,7

Alcalá J.M., Chavarria-K. C., Terranegra L., 1998, A&A 330,1017

D'Antona F., Mazzitelli I., 1994, ApJS 90,467

Babu G.J., Feigelson E.D., 1996, Astrostatistics, Chapman & Hall, London

Bessell M., 1979, PASP 91,589

Blaauw A., 1964, ARAA 2, 213

Blaauw A., 1991, In: Lada C.J., Kylafis N.D. (eds.) The Physics of Star Formation and Early Stellar Evolution, NATO ASI Vol. 342, p. 125

Bildsten L., Brown E.F., Matzner C.D., Ushomirsky G., 1997, ApJ 482,442

Bouvier J., Forestini M., Allain S., 1997, A&A 326,1023

Brandner W., Köhler R., 1998, ApJ 499,L79

Brandner W., Zinnecker H., 1997, A&A 321,220

Brown A.G.A., Dekker G., de Zeeuw P.T., 1997, MNRAS 285,479

Duquennoy A., Mayor M., 1991, A&A 248,485

Elmegreen B.G., Efremov Y., Pudritz R., Zinnecker H., 1999, In: Mannings V. (ed.) Protostars and Planets IV, University of Arizona Press, in press

Feigelson E.D., 1996, ApJ 468,306

Feigelson E.D., Casanova S., Montmerle, T., Guibert J., 1993, ApJ 416, 623

Foster P.N., Boss A.P., 1996, ApJ 468,784

Gagné M., Caillault J.P., Stauffer J.R., 1995, ApJ 445,280

de Geus E.J., 1992, A&A 262,258

de Geus E.J., de Zeeuw P.T., Lub J., 1989, A&A 216,44

Guillout P., Sterzik M.F., Schmitt J.H.M.M., Motch C., Neuhäuser R., 1998, A&A 337,113

Hambly N.C., 1998, The SuperCOSMOS data processing guide, available at http://www.roe.ac.uk/cosmos

Hambly N.C., Miller L., MacGillivray H.T., Herd J.T., Cormack W.A., 1998, MNRAS 298,897

Hartigan P., Strom K.M., Strom S.E., 1994, ApJ 427,961

Herbig G.H., 1962, Adv. Astron. Astrophys., 1,47

Herbig G.H., 1977, ApJ 214,747

Herbig G.H., 1998, ApJ 497,736

Herbig G.H., Bell K.R., 1988, Lick Observatory Bulletin No. 1111

Hillenbrand L.A., Hartmann L.W., 1998, ApJ 492,540

de Jager C., Nieuwenhuijzen H., 1987, A&A 117,217

Kenyon S.J., Hartmann L., 1995, ApJS 101,117

Kenyon S.J., Lada E.A., Barsony M., 1998, AJ 115,252

Kirkpatrick J.D., Kelly D.M., Rieke G.H., et al., 1993, ApJ 402,643

Krautter J., 1991, In: Reipurth B. (ed.) Low Mass Star Formation in Southern Molecular Clouds, ESO Scientific Report No. 11, p. 127

Krautter J., 1996, In: Pallavicini R., Dupree A.K. (eds.) 9th Cambridge Workshop on Cool Stars, Stellar System, and the Sun, ASP Conference Series Vol. 109, p. 395

Krautter J., Wichmann R., Schmitt J.H.M.M., Alcalá J.M., Neuhäuser R., Terranegra L., 1997, A&AS 123,329

Kroupa P., Tout C.A., Gilmore G., 1993, MNRAS 262,545

Kunkel M., 1999, PhD Thesis, Universität Würzburg, (K99)

Lada E.A., Lada C.J., 1995, AJ 109,1682

Lada C.J., Alves J., Lada E.A., 1996, AJ 111,1964

Malkov O., Piskunov A., Zinnecker H., 1998, A&A 338,452

Martin E.L., 1998, AJ 115,351

Martin E.L., Montmerle T., Gregorio-Hetem J., Casanova S., 1998, MNRAS 300,733

Meyer M.R., Wilking B.A., Zinnecker H., 1993, AJ 105,619

Miller G.E., Scalo J.M., 1978, PASP 90,506

Miller G.E., Scalo J.M., 1979, ApJS 41,513

Montmerle T., 1996, In: Pallavicini R., Dupree A.K. (eds.) 9th Cambridge Workshop on Cool Stars, Stellar System, and the Sun, ASP Conference Series Vol. 109, p. 405

Morrison R., McCammon D., 1983, ApJ 270,119

Motte F., André P., Neri R., 1998, A&A 336,150

Neuhäuser R., 1997, Science 276,1363

Neuhäuser R., Preibisch Th., 1995, In: Greiner J., Duerbeck H., Gershberg R.E. (eds.) Flares and Flashes, Proc. of IAU Colloquium 151, Lecture Notes in Physics, Springer Verlag, p. 216

Palla F., Stahler S.W., 1993, ApJ 418,414

Pavlenko Y.V., Magazzu A., 1996, A&A 311,961

Paresce F., 1984, AJ 89,1022

Predehl P., Schmitt J.H.M.M., 1995, A&A 293,889

Preibisch Th., 1997, A&A, 324,690

Preibisch Th., Zinnecker H., Herbig G.H., 1996, A&A 310,456

Preibisch Th., Guenther E., Zinnecker H., Sterzik M., Frink S., Röser S., 1998, A&A 333,619

Raymond J.C., Smith B.W., 1977, ApJS 35,419

Rieke G.H., Lebofsky M.J., 1985, ApJ 288,618

Scalo J.M., 1998, In: Gilmore G., Howel D. (eds.) The stellar intial mass function, ASP Conference Series Vol. 142, p. 201

Sciortino S., Damiani F., Favata F., Micela G., 1998, A&A 332,825

Soderblom D.R., 1996, In: Pallavicini R., Dupree A.K. (eds.) 9th Cambridge Workshop on Cool Stars, Stellar System, and the Sun, ASP Conference Series Vol. 109, p. 315

Soderblom D.R., Jones B.F., Balachandrian S., et al., 1993, AJ 106,1059

Stauffer J., Hartmann L.W., Navascues D.B., 1995, ApJ 454,910

Sterzik M.F., Alcalá J.M., Neuhäuser R., Schmitt J.H.M.M., 1995, A&A 297,418

Walter F.M., Brown A., Mathieu R.D., Myers P.C., 1988, AJ 96,297

Walter F.M., Vrba F.J., Mathieu R.D., Brown A., Myers P.C., 1994, AJ 107,692 (W94)

Walter F.M., Wolk S.J., Freyberg M., Schmitt J.H.M.M., 1997, In: Cool Stars in Clusters and Associations: Magnetic Activity and Age Indicators, eds G. Micela, R. Pallavicini, S. Sciortino, Mem. Soc. Astr. It., Vol. 68, no. 4, p. 1081

Wichmann R., Sterzik M., Krautter J., Metanomski A., Voges W., 1997, A&A 326, 211

Wilking B.A., 1991, In: Reipurth B. (ed.) Low Mass Star Formation in Southern Molecular Clouds, ESO Scientific Report No. 11, p. 159

de Zeeuw P.T., Brand J., 1985, In: van den Woerden H., Boland W. (eds.) Birth and Evolution of Massive Stars and Stellar Groups, Reidel, Dordrecht, p. 95

de Zeeuw P.T., Hoogerwerf R., de Bruijne J.H.J., Brown A.G.A., Blaauw A., 1999, AJ 117,354

Zinnecker H., McCaughrean M.J., Wilking B.A., 1993, In: Levy E.H., Lumine J.I. (eds.) Protostars and Planets III, University of Arizona Press, p. 429

This 2-column preprint was prepared with the AAS LaTeX macros v4.0.

Table 1: PMS stars in Upper Sco. The source name in the first column consists of the J2000 coordinates of the star. The second column denotes the study in which the PMS star was identified. The third column contains the spectral type, the fourth column tells whether the star was detected in the RASS ("R") and whether it was selected as a candidate for a PMS star ("C") or as a non-PMS candidate ("nC"). The other colums give photometric data and stellar parameters.

USco		SpT	RASS	B	I	$R-I$	A_V	$\log T_{\rm eff}$	$\log \frac{L}{L_\odot}$	$M_\star$	age
				[mag]	[mag]	[mag]	[mag]	[K]		[$M_\odot$]	[Myr]
153557.8−232405	P98	K3:	RC	13.1	10.88	0.86	1.4	3.649	−0.118	0.90	3.0
154106.7−265626	P98	G7	RC	12.6	9.98	0.77	1.6	3.701	0.258	1.42	3.0
154413.4−252258	P98	M1	RC	14.4	11.33	1.13	0.6	3.564	−0.431	0.38	1.0
154920.9−260005	K99	K0	RC	11.7	9.71	0.64	0.7	3.676	0.208	1.10	1.8
155106.6−240218	K99	M2	RC	15.1	12.08	1.19	0.4	3.551	−0.759	0.35	2.5
155231.2−263351	K99	M0	RC	13.1	10.88	0.75	0.0	3.576	−0.372	0.43	1.0
155459.9−234718	W94	G2	RnC	9.3	8.14	0.41	0.2	3.738	0.722	1.82	2.8
155506.2−252109	K99	M1	RnC	13.5	10.57	0.86	0.0	3.564	−0.241	0.33	0.6
155517.1−232216	W94	M2.5		15.2	12.17	1.11	0.0	3.545	−0.863	0.30	2.9
155548.7−251223	K99	G3	RC	10.6	9.44	0.42	0.2	3.731	0.200	1.34	9.0
155702.3−195042	P98	K7:	RC	12.7	10.24	0.77	0.2	3.609	−0.080	0.50	0.8
155716.6−252918	K99	M0		13.7	10.94	0.85	0.0	3.576	−0.396	0.44	1.2
155720.0−233849	W94	M0		13.7	10.95	0.92	0.0	3.576	−0.397	0.44	1.2
155725.8−235422	W94	M0.5		14.6	10.94	1.16	0.9	3.570	−0.210	0.34	0.5
155734.4−232111	W94	M1	RC	14.3	11.37	1.18	0.8	3.564	−0.401	0.38	0.9
155750.0−230508	K99	M0	RC	14.4	11.46	0.95	0.1	3.576	−0.574	0.50	2.9
155812.7−232835	K99	G2	RnC	10.9	9.25	0.47	0.4	3.738	0.333	1.47	8.0
155847.8−175800	P98	K3	RC	12.9	10.46	0.94	1.8	3.649	0.123	0.78	1.0
155902.1−184414	P98	K6	RC	13.0	10.40	0.94	1.3	3.620	0.053	0.53	0.7
155950.0−255557	K99	M2	RC	14.3	11.89	1.31	1.0	3.551	−0.573	0.35	1.5
160000.0−222037	W94	M1		14.0	11.08	1.13	0.6	3.564	−0.331	0.36	0.8
160000.7−250941	K99	G0	RnC	10.9	9.69	0.36	0.0	3.750	0.080	1.10	18.0
160013.3−241810	K99	M0		14.6	11.68	1.04	0.6	3.576	−0.580	0.50	3.0
160031.3−202705	K99	M1		14.8	11.24	1.22	1.0	3.564	−0.313	0.35	0.7
160040.6−220032	K99	G9	RC	12.1	9.95	0.56	0.5	3.685	0.053	1.22	4.0
160042.8−212737	K99	K7		14.2	10.97	0.88	0.8	3.609	−0.272	0.60	1.8
160105.2−222731	W94	M3		14.3	11.27	1.33	0.5	3.538	−0.398	0.27	0.5
160108.0−211318	K99	M0	RC	13.9	10.86	0.86	0.0	3.576	−0.364	0.42	1.0
160125.7−224040	W94	K1	RC	12.0	10.16	0.63	0.6	3.667	0.002	1.05	3.0
160147.4−204945	K99	M0	RnC	14.3	10.92	1.08	0.8	3.576	−0.239	0.38	0.8
160151.4−244524	K99	K7	RC	13.4	10.54	0.84	0.6	3.609	−0.136	0.53	1.0
160158.2−200811	K99	G5	RC	11.2	9.29	0.58	0.8	3.717	0.383	1.60	3.3
160200.3−222123	K99	M1	RC	14.9	11.23	1.23	1.1	3.564	−0.300	0.35	0.8
160208.5−225457	W94	M1		15.7	11.91	1.13	0.6	3.564	−0.663	0.43	2.8
160210.4−224128	W94	K5	RC	11.9	9.89	0.71	0.4	3.630	0.083	0.60	0.7
160239.1−254208	P98	K7	RC	13.2	10.80	0.73	0.0	3.609	−0.341	0.65	2.7
160251.2−240156	K99	K4	RC	13.2	10.82	0.71	0.6	3.639	−0.257	0.90	4.0
160253.9−202248	K99	K7	RC	13.4	10.58	0.96	1.1	3.609	−0.043	0.50	0.8
160302.7−180605	P98	K4	RC	12.8	10.78	0.83	1.1	3.639	−0.132	0.80	2.2
160323.7−175142	P98	M2	RC	14.3	11.06	1.25	0.7	3.551	−0.296	0.30	0.4

Table 1: − continued

USco		SpT	RASS	B [mag]	I [mag]	$R-I$ [mag]	A_V [mag]	$\log T_{\rm eff}$ [K]	$\log \frac{L}{L_\odot}$	$M_\star$ [$M_\odot$]	age [Myrs]
160354.9−203137	K99	M0	RC	14.0	11.10	1.10	0.9	3.576	−0.293	0.40	0.9
160357.6−203105	K99	K5	RC	13.4	10.92	0.81	0.9	3.630	−0.237	0.78	2.9
160420.9−213042	K99	M2	RC	16.6	12.13	1.57	2.2	3.551	−0.431	0.33	0.9
160421.7−213028	K99	K2	RC	13.3	10.64	0.73	1.0	3.658	−0.118	1.00	3.7
160447.7−193023	W94	K2	RC	12.2	9.82	0.65	0.6	3.658	0.137	0.90	1.2
160527.3−193846	W94	M1		15.5	11.99	1.07	0.3	3.564	−0.750	0.44	3.5
160539.1−215230	K99	M1		15.8	11.93	1.18	0.8	3.564	−0.625	0.43	2.5
160542.7−200415	W94	M2	RC	15.0	11.76	1.34	1.1	3.551	−0.494	0.34	1.0
160550.5−253313	P98	G7	RC	11.7	9.99	0.47	0.2	3.701	−0.019	1.20	8.5
160612.5−203647	K99	K5	RC	14.0	11.27	1.00	1.8	3.630	−0.203	0.75	2.5
160621.9−192844	W94	M0.5	RC	14.1	11.33	1.09	0.6	3.570	−0.430	0.41	1.1
160637.4−210840	K99	M1	RC	15.1	11.67	1.33	1.5	3.564	−0.384	0.37	0.9
160639.9−200128	W94	M3		16.8	12.79	1.43	1.0	3.538	−0.915	0.27	2.8
160654.4−241610	P98	M3	RC	13.8	10.87	1.08	0.0	3.538	−0.335	1.05	3.0
160703.5−203626	K99	M0	RC	14.3	10.22	0.90	0.0	3.576	−0.108	0.33	0.5
160703.6−204308	K99	M1		16.0	12.15	1.22	1.0	3.564	−0.677	0.43	2.8
160703.9−191132	K99	M1	RC	15.0	11.81	1.23	1.1	3.564	−0.532	0.40	1.7
160814.7−190833	P98	K2	RC	12.2	10.28	0.87	1.6	3.658	0.154	0.87	1.2
160831.4−180241	P98	M0	RC	14.0	11.26	0.93	0.1	3.576	−0.512	0.47	2.0
160843.4−260216	P98	G7	RC	11.1	9.30	0.71	1.3	3.701	0.476	1.50	1.8
160856.7−203346	P98	K5	RC	13.3	10.86	0.92	1.4	3.630	−0.113	0.70	1.8
160930.3−210459	P98	M0	RC	13.8	11.14	0.81	0.0	3.576	−0.476	0.47	2.0
160941.0−221759	P98	M0	RC	13.8	11.06	0.84	0.0	3.576	−0.444	0.45	1.8
161019.1−250230	P98	M1	RC	13.0	9.76	1.01	0.0	3.564	0.087	0.28	0.1
161021.7−190406	W94	M1	RnC	15.0	12.26	1.45	2.1	3.564	−0.511	0.40	1.8
161028.5−190446	W94	M3		14.5	11.42	1.27	0.2	3.538	−0.513	0.28	0.9
161042.0−210132	P98	K5	RC	13.4	10.74	0.94	1.5	3.630	−0.046	0.66	1.1
161108.9−190446	W94	K2	RC	12.4	10.17	0.89	1.7	3.658	0.216	0.84	1.0
161120.6−182054	W94	K5	RnC	13.2	10.73	0.83	1.0	3.630	−0.143	0.70	1.8
161156.3−230404	P98	M1	RC	14.2	10.91	1.18	0.8	3.564	−0.217	0.32	0.5
161159.2−190652	W94	K0	RC	12.0	10.18	0.75	1.3	3.676	0.120	1.12	2.5
161220.9−190903	W94	M2.5		15.5	12.68	1.36	0.9	3.545	−0.888	0.30	3.0
161240.5−185927	W94	K0	RC	12.6	9.38	0.72	1.1	3.676	0.413	1.01	0.8
161302.7−225744	P98	K4	RC	12.6	10.38	1.08	2.3	3.639	0.257	0.64	0.5
161318.6−221248	P98	G9	RC	11.3	9.25	0.66	0.9	3.685	0.425	1.18	1.0
161329.3−231106	P98	K1	RC	12.5	10.29	0.92	2.0	3.667	0.215	0.95	1.2
161402.1−230101	P98	G4	RC	12.2	10.06	0.81	2.0	3.724	0.297	1.50	5.0
161411.0−230536	P98	K0	RC	11.5	9.19	0.99	2.4	3.676	0.736	1.02	0.3
161459.2−275023	P98	G5	RC	11.8	10.11	0.61	1.0	3.717	0.083	1.28	9.0
161534.6−224241	P98	M1	RC	13.2	10.38	1.06	0.3	3.564	−0.115	0.29	0.3
161618.0−233947	P98	G7	RC	11.3	9.55	0.67	1.1	3.701	0.339	1.47	2.2
161731.4−230334	W94	G0	RC	10.3	9.14	0.47	0.5	3.750	0.400	1.43	9.0
161933.9−222828	P98	K0	RC	12.0	10.09	0.75	1.3	3.676	0.156	1.10	2.0
162046.0−234820	P98	K3	RC	13.4	10.70	1.03	2.2	3.649	0.109	0.78	1.0
162307.8−230059	P98	K2	RC	12.7	10.18	0.69	0.8	3.658	0.029	0.93	2.0
162948.6−215211	W94	K0	RC	11.9	9.77	0.71	1.1	3.676	0.248	1.08	1.8

Table 2: Results of our binary simulations.

$M_{\rm p}/M_\odot$	$\langle\Delta\log L\rangle$	$Q_{90}(\Delta\log L)$	$\max(\Delta\log L)$
2.5	0.012	0.020	0.301
2.0	0.022	0.045	0.301
1.8	0.033	0.074	0.301
1.6	0.057	0.128	0.301
1.4	0.089	0.199	0.301
1.2	0.123	0.260	0.301
1.0	0.154	0.298	0.303
0.8	0.181	0.313	0.318
0.6	0.210	0.321	0.326
0.4	0.249	0.316	0.319
0.2	0.300	0.304	0.304
0.15	0.312	0.319	0.320

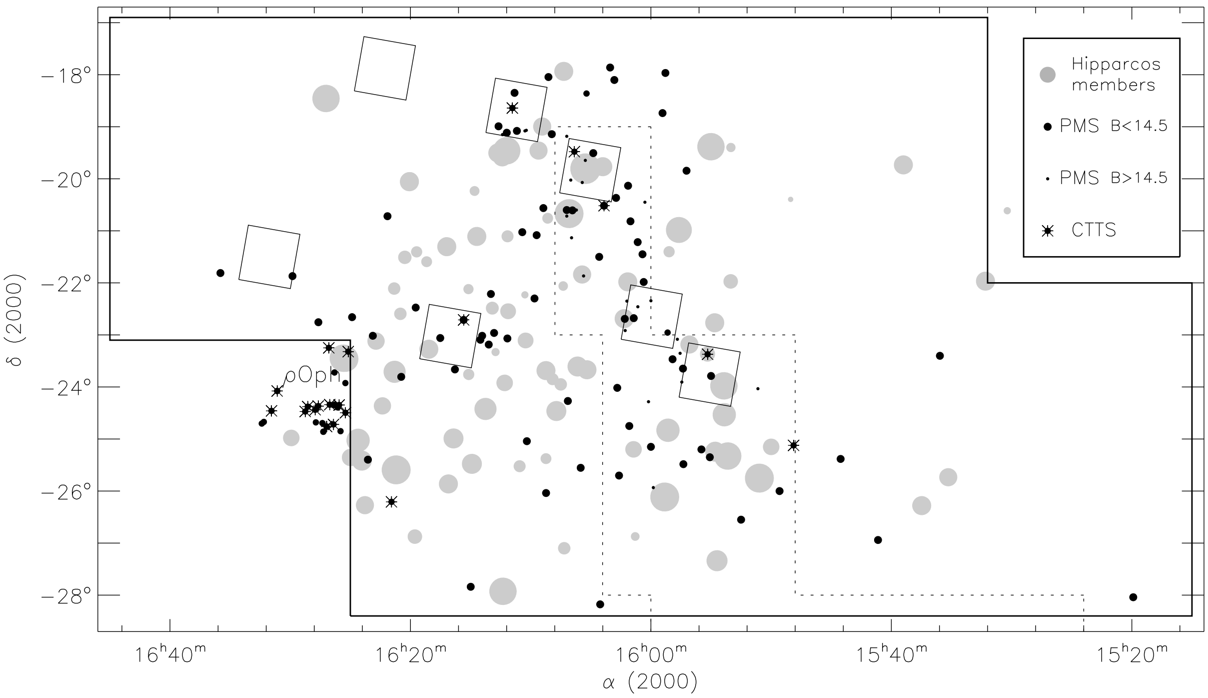

Fig. 1.— Map of our field in Upper Sco region, marked by the thick solid line. The relatively bright ($B < 14.5$) low-mass PMS stars, for which our sample is spatially unbiased, are shown as big solid dots, the fainter PMS stars as small solid dots, and classical T Tauri stars are marked with asterisks. The Hipparcos high-mass members are shown as big grey dots, with symbol size proportional to the logarithm of their luminosity. The squares show the EINSTEIN fields investigated by W94, the dotted line marks the region studied by K99.

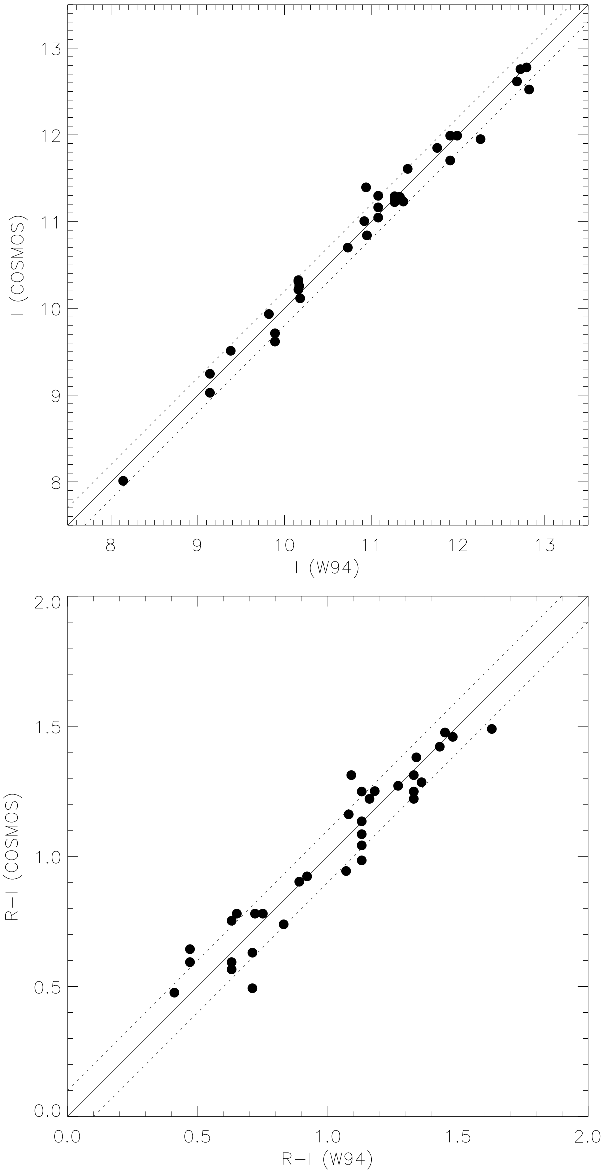

Fig. 2.— I magnitudes and $R-I$ colors derived from the COSMOS magnitudes compared to the photoelectric magnitudes of W94. The dotted lines define the ± 0.2 mag band for I and the ± 0.1 mag band for $R-I$.

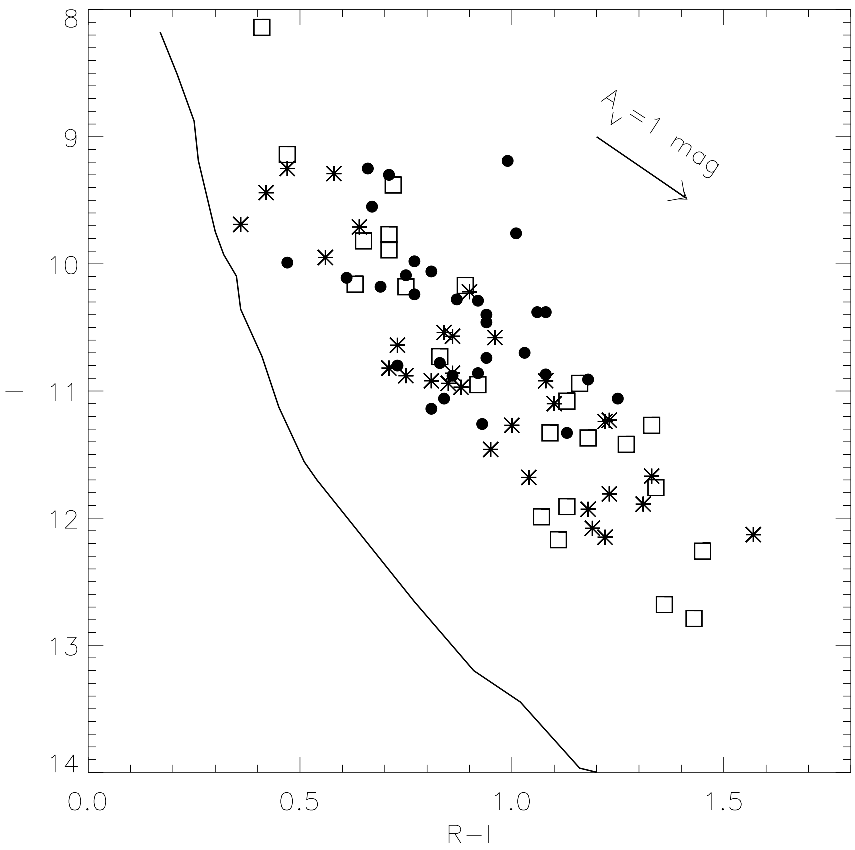

Fig. 3.— Color-Magnitude diagram for our sample of PMS stars in Upper Sco. The PMS stars from W94 are shown as boxes, those of K99 as asterisks, and those of P98 as solid dots. The line shows the main sequence.

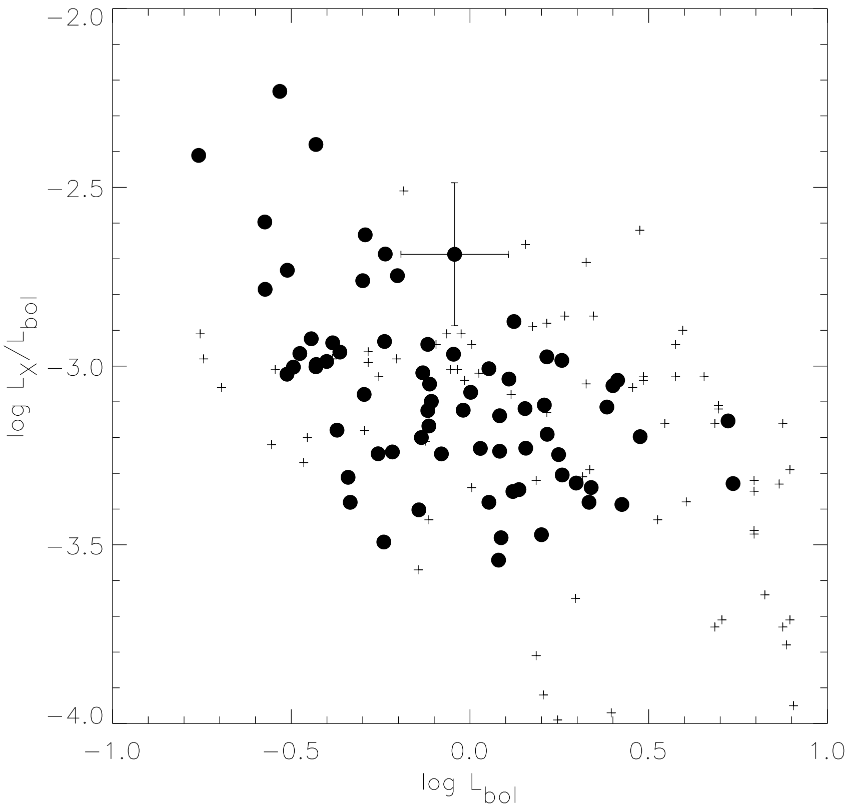

Fig. 4.— Fractional X-ray luminosities and bolometric luminosities of the PMS stars in Upper Sco are shown as big solid dots. Typical error bars are shown for one star. The small crosses show data for T Tauri stars in the Orion Nebula from Gagné et al. (1995). The objects with the highest fractional X-ray luminosities ($\log{(L_{\rm X}/L_{\rm bol})} \gtrsim -2.5$) were probably flaring during the X-ray observations.

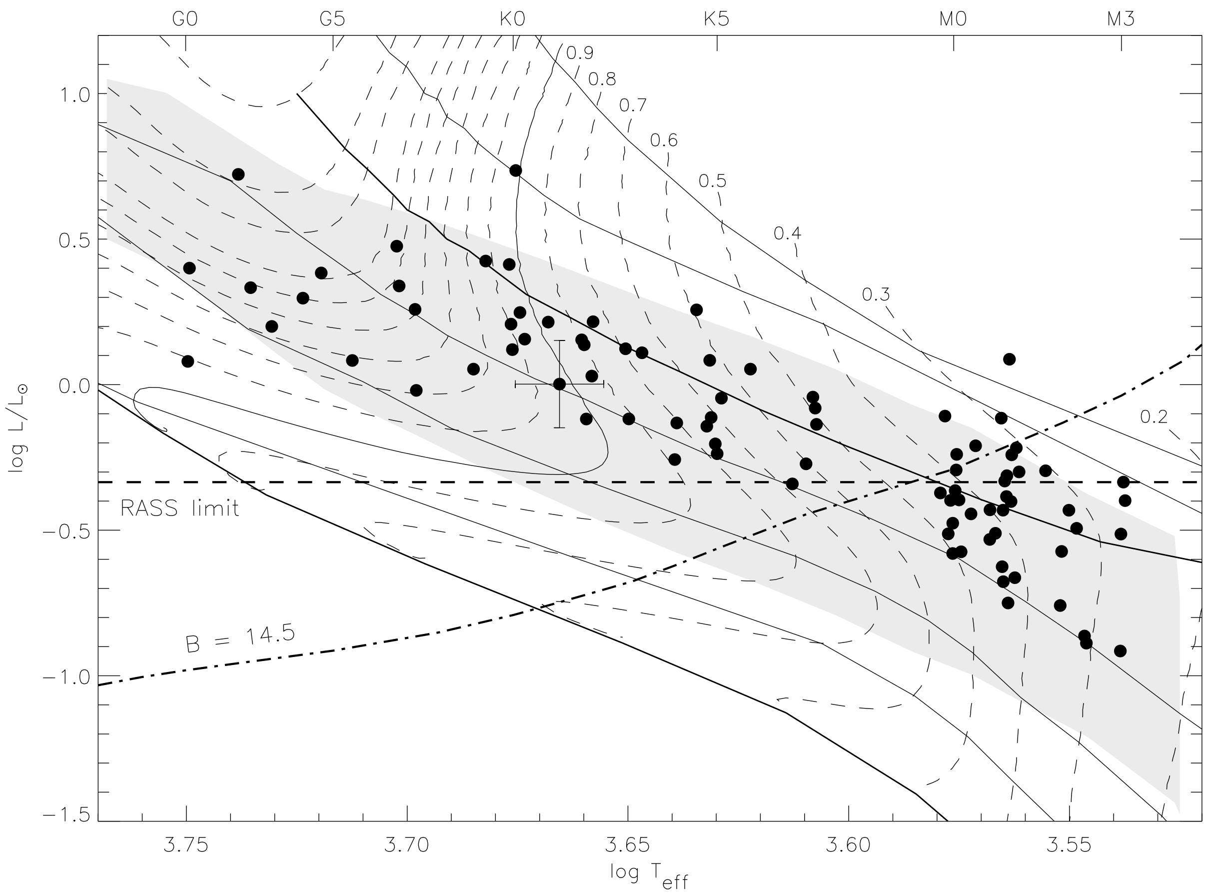

Fig. 5.— HR diagram for the PMS stars in Upper Sco. The PMS stars are shown as solid dots, the dashed lines show the evolutionary tracks from DM94; the 1 $M_\odot$ track is shown as a solid line, the low-mass tracks are labeled by their masses. The solid lines show the DM94 isochrones for the ages of 0.1, 0.3, 1 (thick line), 3, 10, and 30 Myr and finally the main sequence. The grey shaded band shows the region in which we expect 90% of the PMS stars to lie, based on the assumption of a common age of 5 Myr for all stars and taking proper account of the uncertainties and the effects of unresolved binaries (for details see text). The thick horizontal dashed line indicates the sensitivity limit of the X-ray observations, the thick dashed-dotted line indicates the magnitude limit of the FLAIR observations of P98. For one of the PMS stars typical error bars are shown.

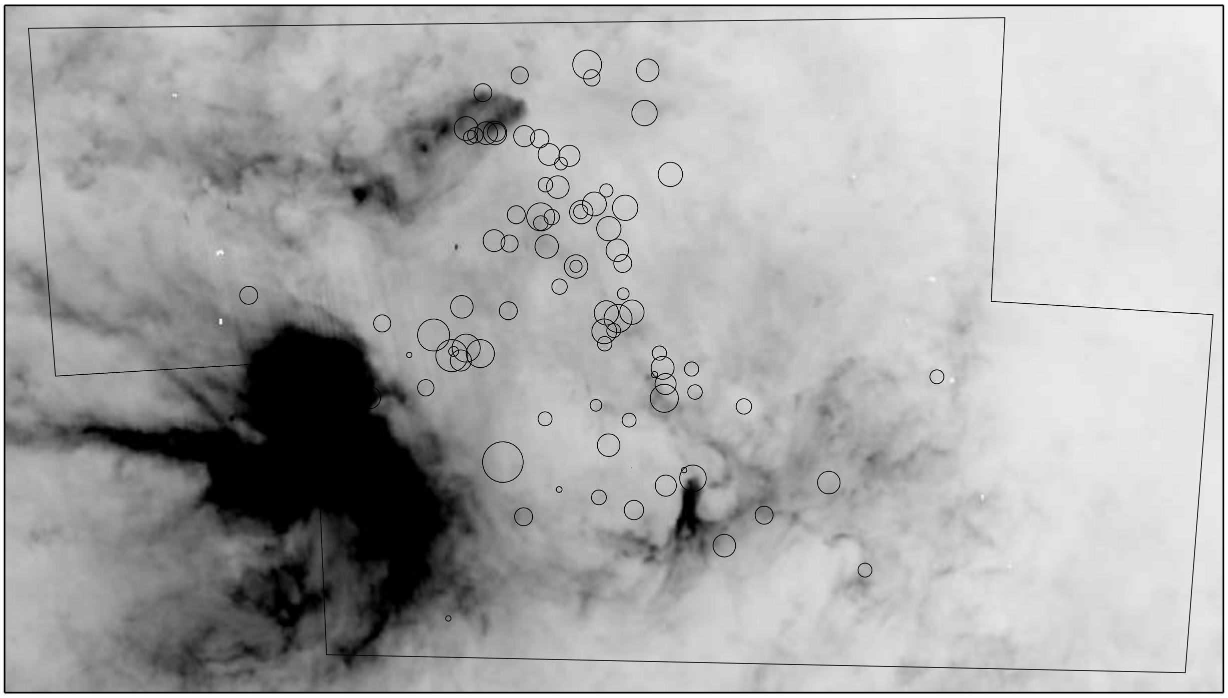

Fig. 6.— IRAS 100 μm map of the Upper Scorpius region, displayed with an inverse linear greyscale ranging from $0 - 150$ MJy/sr. The positions of the PMS stars are marked by circles. Symbol size is a measure of isochronal age: the stars with the youngest isochronal ages are marked by the largest symbols, those with the oldest isochronal ages by the smallest symbols.

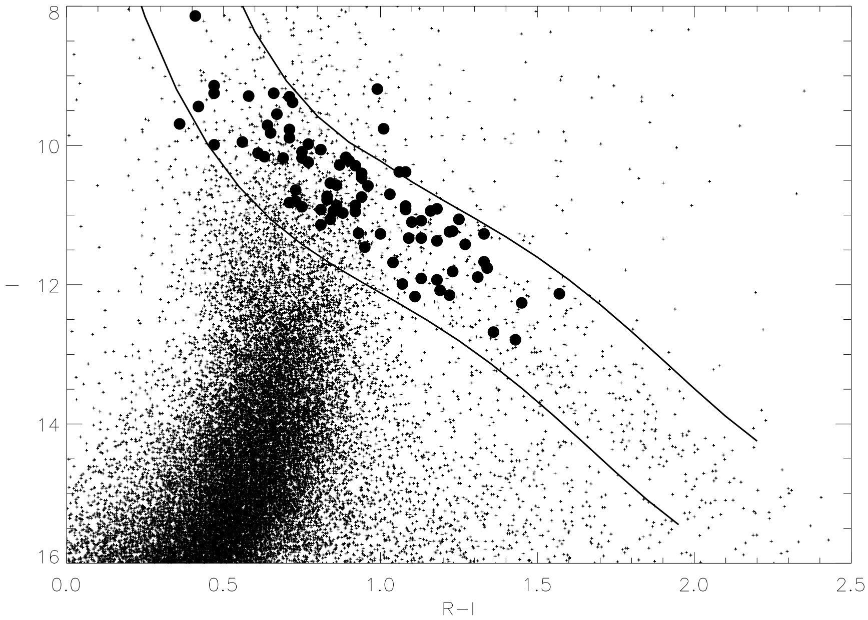

Fig. 7.— Color-Magnitude diagram for all stars (small crosses) in a 12 square-degree area near the center of our field. The known PMS stars in Upper Sco are shown by the big solid dots. The lower solid line shows the theoretical 5 Myr isochrone, together with the upper line it denotes the band of photometric candidate PMS stars.

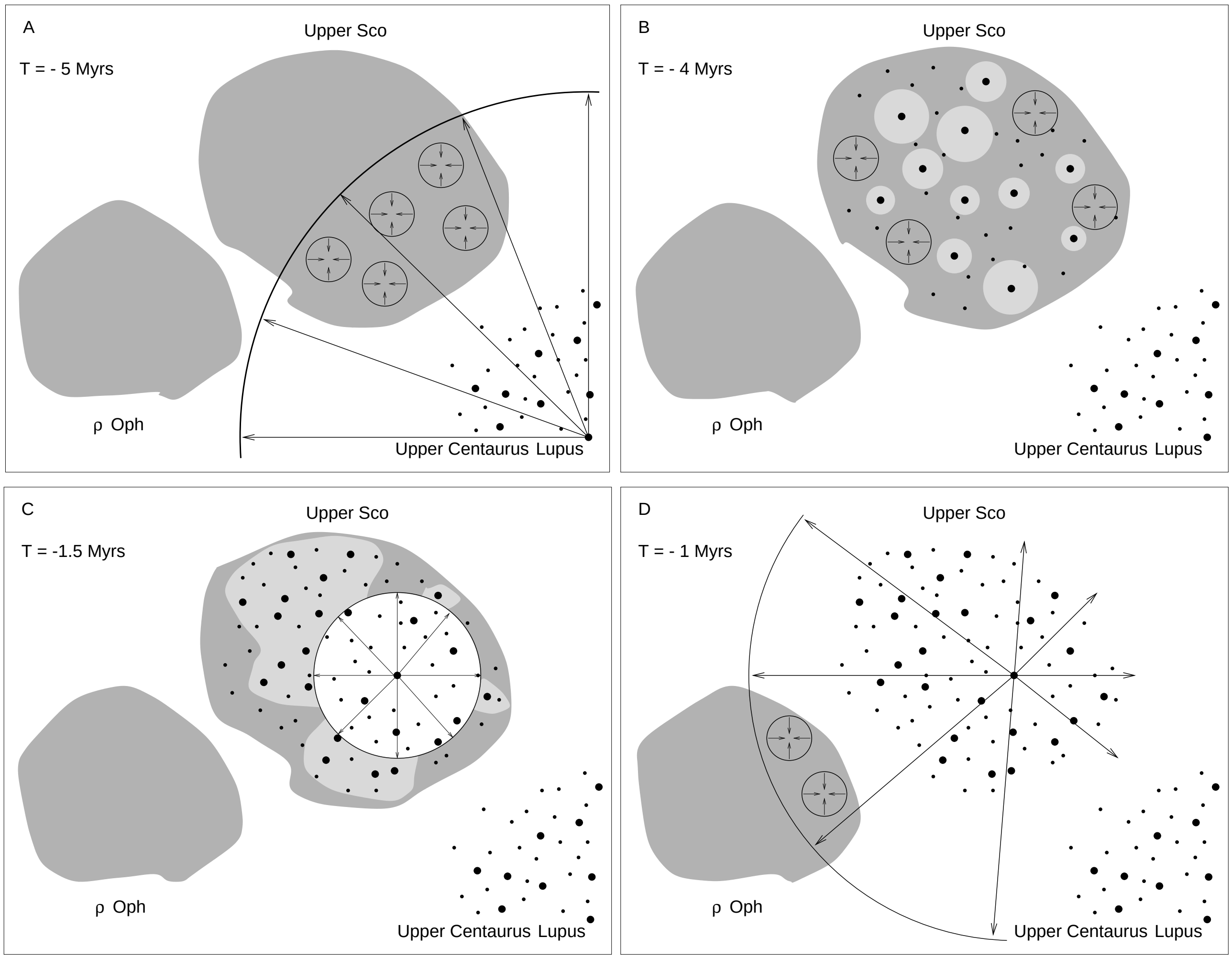

Fig. 8.— Schematic view of the star formation history in the Scorpius-Centaurus association. Molecular clouds are shown as dark regions, high-mass and low-mass stars as large resp. small dots. For further details on the sequence of events see section 9.2.